IAC-13,C1,9,6,x18172

APPLICATIONS OF SOLAR RADIATION PRESSURE DOMINATED HIGHLY NON-KEPLERIAN TRAJECTORIES AROUND MINOR BODIES

D. García Yárnoz,
Advanced Space Concepts Laboratory, University of Strathclyde, UK, daniel.garcia-yarnoz@strath.ac.uk

J.P. Sanchez Cuartielles*
Advanced Space Concepts Laboratory, University of Strathclyde, UK, jpau.sanchez@upc.edu

C.R. McInnes
Advanced Space Concepts Laboratory, University of Strathclyde, UK, colin.mcinnes@strath.ac.uk

With the growing interest in the exploration and possible exploitation of small minor bodies, demonstrator missions to asteroids and comets are a trending topic in the research community. Various strategies appearing in literature for the characterisation and proximity operations of small asteroids have limited coverage of the sunlit side of an asteroid. This paper proposes the use of highly non-Keplerian trajectories enabled by solar radiation pressure to map and characterize the region around the sub-solar point of small asteroids. Strategies involving a combination of retrograde and prograde orbits together with inversions of the orbit direction by either manoeuvres or exploiting the natural dynamics are presented and analysed in detail. Additional orbits of interest for hopper spacecraft are also discussed.

I. INTRODUCTION

In the low gravity environments of small asteroids, the solar radiation pressure (SRP) perturbation becomes the largest non-gravitational force affecting the orbital motion of a spacecraft in the vicinity of an asteroid. For large asteroids, such as Eros and Vesta, relatively stable orbiting regimes can be achieved (Scheeres, 1994, Scheeres et al., 2003). This is not the case for much smaller objects (of a diameter of less than a few hundreds of meters), where SRP destabilizes most orbits. The well-known terminator orbits (Dankowicz, 1993, Scheeres, 2007, Byram and Scheeres, 2008) have been proposed for spacecraft orbiting these bodies. They are the only long-term quasi-stable orbits around asteroids when SRP is dominant. Most other bound orbits experience great excursions in eccentricity, which cause them to re-impact or escape after a small number of revolutions. However, these other orbits are not completely devoid of interest and will be the focus of this paper.

One of the main drawbacks of terminator orbits is precisely the limited coverage that they provide of the asteroid. Because of their definition, on the terminator and slightly displaced towards the dark side, their observation of the features of the asteroid is limited to the terminator line, which implies long shadows and it is not optimal for optical observations. The sub-solar point and other areas with direct sunlight are not accessible, as well as the anti-solar point.

The possibility of orbits close to the Lagrangian L_1 point is discarded. The SRP perturbation displaces the L_1 point by a large distance towards the Sun, and so it is not suitable for close observations.

Various solutions to this problem have already been studied in literature. Using the classical Stark problem, it was demonstrated that trajectories remain confined between paraboloids when small perturbations are applied to terminator orbits (Bookless and McInnes, 2006, Bookless, 2006). One set of paraboloids extends towards the sun direction, which would allow partial coverage of the sun-lit side of the asteroid, while the second set extends towards the anti-Sun direction. One subset of these type of orbits, a family of periodic orbits confined to the Sun direction paraboloid, were proposed in Broschart et al. (2013) to provide partial coverage of the sunlit side. They termed these trajectories quasi-terminator orbits (QTO), as they extend the terminator orbit they originate from towards the sun-lit side. However, the coverage of the sub-solar point is still limited.

Other solutions to the sub-solar point coverage include direct hovering in a quasi inertial frame or co-rotating frame (Broschart and Scheeres, 2005, Broschart and Scheeres, 2007), or pseudo-hovering solutions where the spacecraft stays in a control box, with regular manoeuvres reversing the velocity vector (Scheeres, 2012). Because of the cost of orbit maintenance, these solutions are feasible for small asteroids only.

* Currently at Universitat Politècnica de Catalunya, Spain

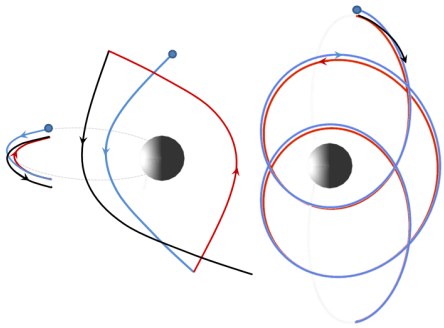

Figure 1: Schematic representation of sub-solar point mapping strategies: control box pseudo-hovering scheme and multiple low-velocity flybys (left), and the proposed SRP enabled alternating orbiter (right).

Another possible strategy is the use of multiple low-velocity flybys of the asteroid (Takahashi and Scheeres, 2011). This was suggested as a means to characterise the gravity field of a small asteroid without inserting into orbit, but it could also be used for monitoring various regions of interest on the surface of an asteroid.

An intermediate strategy between control box hovering and multiple flybys is here proposed: an alternating orbiter in which the spacecraft stays in orbit around the asteroid performing regular manoeuvres to reverse the velocity vector and orbit direction after a few revolutions. These inversions are intended to avoid re-impact due to the increase in eccentricity caused by SRP. On one hand, the cost for orbit maintenance for this strategy is expected to be lower than hovering solutions previously investigated. In addition, having an orbiting solution will allow for a faster characterisation of the gravity field, and more comprehensive coverage than multiple flybys.

In order to identify feasible orbits for the proposed strategy, this paper therefore analyses the evolution of eccentricity and orbit orientation of a high-area-to-mass ratio spacecraft on a plane perpendicular to the terminator. The dynamical models implemented are first described. With the application of these models, multiple revolutions, direct re-impact, orbit direction inversions or escape trajectories are among the possible orbiting regimes enabled by the SRP perturbation. Novel solutions for these highly non-Keplerian orbits to be used for scientific exploration are sought and are here then presented.

II. THE PHOTO-GRAVITATIONAL CIRCULAR RESTRICTED 3-BODY PROBLEM (CR3BP)

For the solar radiation pressure acting on the spacecraft the standard cannon-ball model is assumed:

$$\bar{F}_{SRP} = \frac{LQA}{4\pi c}\frac{\vec{r}_{S-SC}}{\left|\vec{r}_{S-SC}\right|^3} \tag{1}$$

where L is the solar luminosity, Q the solar radiation pressure coefficient, which depends on the reflectivity of the surface, A the cross-sectional area of the spacecraft, c is the speed of light and $\vec{r}_{S-SC}$ is the radius-vector from the Sun to the spacecraft. This assumes the SRP force has only a radial component, with the effective surface of the spacecraft perpendicular to the Sun-spacecraft line. The solar radiation pressure coefficient is 1 for a perfectly absorbing surface, and is equal to 2 for the case of ideal specular reflection. Unless otherwise stated, for the analysis in this paper the conservative value of Q=1 is assumed.

Both the SRP force and the gravitational attraction of the Sun scale with the inverse of the distance squared. The ratio between both forces defines the lightness number β given by:

$$\beta = \frac{LQ}{4\pi c \mu_S}\frac{A}{m} \tag{2}$$

where μ_S is the gravitational constant of the Sun. It is proportional to the area-to-mass ratio, and both the lightness number β and the cross-sectional area A (once the spacecraft mass is fixed) will be used interchangeably in the paper to describe the different orbiting regimes.

With this SRP model, the behaviour of the system can be described with the well-known photo-gravitational circular restricted three-body problem (Chernikov, 1970, Schuerman, 1980, Simmons et al., 1985), applied to a hypothetical asteroid in a circular orbit at 1AU around the Sun:

$$\begin{cases} \ddot{x} - 2\Omega_R \dot{y} = \Omega_R{}^2\left(x - \frac{(1-\mu)(1-\beta)(x+\mu)}{\left((x+\mu)^2+y^2+z^2\right)^{3/2}} - \frac{\mu(x+\mu-1)}{\left((x+\mu-1)^2+y^2+z^2\right)^{3/2}} \right) \\ \ddot{y} + 2\Omega_R \dot{x} = \Omega_R{}^2\left(y - \frac{(1-\mu)(1-\beta)y}{\left((x+\mu)^2+y^2+z^2\right)^{3/2}} - \frac{\mu y}{\left((x+\mu-1)^2+y^2+z^2\right)^{3/2}} \right) \\ \ddot{z} = \Omega_R{}^2\left(-\frac{(1-\mu)(1-\beta)z}{\left((x+\mu)^2+y^2+z^2\right)^{3/2}} - \frac{\mu z}{\left((x+\mu-1)^2+y^2+z^2\right)^{3/2}} \right) \end{cases} \tag{3}$$

$$\mu = \frac{\mu_A}{\mu_A+\mu_S}; \quad \Omega_R = \sqrt{\frac{\mu_A+\mu_S}{\left|r_{S-A}\right|^3}}$$

where distances have been normalised with respect to the Sun-asteroid distance $\left|r_{S-A}\right|$ (equal to 1 AU in this case), μ_A is the gravitational parameter of the asteroid, and Ω_R is the frequency of rotation of the two bodies around the barycentre. The state vectors are given in a co-rotating frame with the origin at the barycentre of the system and the x-axis pointing towards the asteroid (see Figure 2).

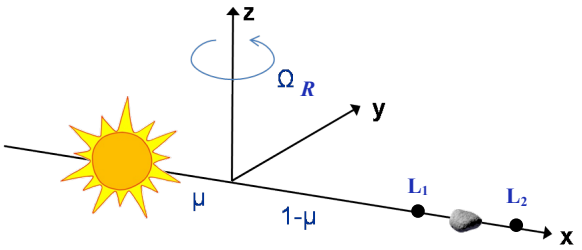

Figure 2: Schematic representation of the co-rotating frame centred in the barycentre of the Sun-asteroid system.

III. HAMILTONIAN APPROXIMATION

In order to study circumplanetary dust dynamics in a planar equatorial case, Hamilton and Krikov (1996) proposed a method based on orbit-averaging Lagrange's planetary equations over one revolution. This method was later used by various authors to describe applications for high-area-to-mass ratio spacecraft for Earth geo-magnetic tail exploration (McInnes et al., 2001, Oyama et al., 2008), passive de-orbiting, and heliotropic orbit applications (Colombo et al., 2011).

They demonstrated that the dynamics of high-area-to-mass ratio objects can be easily described in an eccentricity-phase angle space, with the phase angle ϕ defined by:

$$\phi = \Omega + \arctan\left(\frac{\cos i \sin\omega}{\cos\omega}\right) - \lambda_{SUN} + \pi \tag{4}$$

where Ω represents the right ascension of the ascending node of the orbit around the planet (or in our case asteroid), i and ω are the inclination and argument of the pericentre, and λ_{SUN} is the solar longitude (see Figure 3).

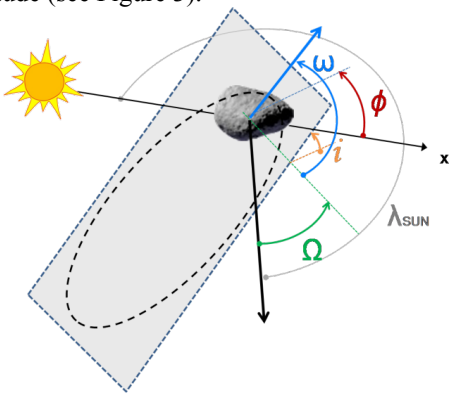

Figure 3: Definition of the phase angle ϕ

It follows from their analysis that the evolution of e and ϕ is along isolines of constant Hamiltonian, with the Hamiltonian and governing equations given by:

$$H = \sqrt{1-\bar{e}^2} + \frac{1}{2}B\bar{e}^2\left(1+5\cos(2\phi)\right) - C\bar{e}\cos\phi$$

$$C = \frac{3}{2}\beta\sqrt{\frac{\mu_S}{\mu_A}\frac{\bar{a}}{|r_{S-A}|}} \qquad B = \frac{3}{4}\sqrt{\frac{\mu_S}{\mu_A}\frac{\bar{a}^3}{|r_{S-A}|^3}} \tag{5}$$

$$\begin{cases} \dfrac{\partial\bar{e}}{\partial\lambda_{SUN}} = -\dfrac{\sqrt{1-\bar{e}^2}}{\bar{e}}\dfrac{\partial H}{\partial\phi} \\ \dfrac{\partial\phi}{\partial\lambda_{SUN}} = \dfrac{\sqrt{1-\bar{e}^2}}{\bar{e}}\dfrac{\partial H}{\partial\bar{e}} \end{cases}$$

with terms accounting for the influence of SRP (C) and the tidal forces induced by third body perturbation of the Sun (B). The eccentricity and semi-major axis are orbit averaged values. It can also be demonstrated that the variation of semi-major axis over one revolution is zero.

Contrary to the cases investigated around Earth, there are no equilibrium points in the Hamiltonian for the considered case of high SRP around a small asteroid. The Hamiltonian isolines all reach at some point the critical eccentricity value of 1 (representing a parabolic orbit), which results in all trajectories either escaping or impacting the surface eventually. The shape of the isolines is represented in Figure 4 for a prograde orbit (i.e. rotating counter-clockwise), with the eccentricity decreasing for phase angles lower than 180 degrees, and increasing for phase angles larger than 180. This implies that there are orbits or trajectories that starting with very high eccentricities, due to the effect of SRP become almost circular before the eccentricity grows again back to values close to 1. For retrograde orbits (rotating clockwise) the phase space would be flipped horizontally with respect to $\phi = 180^0$, and the direction of the isolines is reversed.

The graph also indicates a critical eccentricity (horizontal line) above which all pericentres are below the asteroid surface. This critical eccentricity varies along the orbit with the osculating semi-major axis. If there is a pericentre passage above this line it implies a re-impact with the asteroid. If instead no pericentre passage takes place, the eccentricity can grow up to values greater than 1, and so the resulting trajectory corresponds in principle to an escape trajectory.

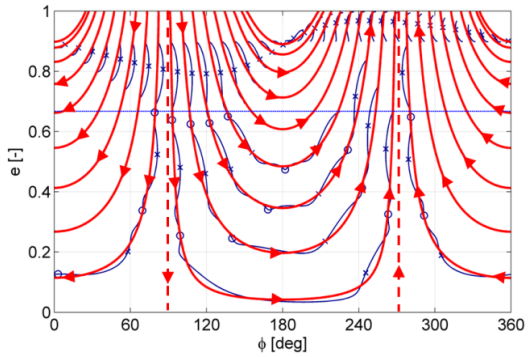

Figure 4: Eccentricity-ϕ plot comparing numerical propagated trajectories (thin blue lines) and the isolines of constant Hamiltonian (thick red lines). Apocentres and pericentres of the numerical trajectories are indicated with X and O respectively.

In the following sections, only full numerical propagation of trajectories will be considered. However, the phase space plots of the averaged Hamiltonian approach still provide an intuitive analytical explanation for the evolution of the orbital elements in a high-SRP and low gravity environment. Phase space graphs of the numerical trajectories will be plotted in order to understand the different orbiting regimes, and to observe the deviations with respect to the expected analytical behaviour. In most cases the trajectories studied in this paper will have initial phase angle ϕ of 90 or 270 degrees (vertical dashed isolines in Figure 4), which corresponds to orbits with the initial pericentre on the positive or negative Y-axis. They are of particular interest as the eccentricity reaches smaller values close to 0 (circular orbits) and as a general rule tend to remain longer in orbit (they require more time for the eccentricity to grow back to critical values).

IV. NUMERICAL MODEL

Trajectories have been numerically propagated using the equations of the photo-gravitational CR3BP presented in Eq. (3), with some modifications to include the effect of eclipses and non-sphericity of the asteroid.

IV.I. Eclipses

The original definition of the photo-gravitational CR3BP and the Hamiltonian approach do not take eclipses into account. For the trajectories considered in this paper, eclipses, though short in duration, have a significant effect on the evolution of orbits.

Eclipses have thus been included in the numerical propagation in two different ways. A first simple approximation is to model them as a cylindrical shadow projected by a spherical asteroid of radius R, and assuming the lightness number becomes zero whenever the eclipse conditions are satisfied:

$$\begin{cases} \vec{r}\cdot\vec{r}_{S-A} > 0 \\ \left| \vec{r}\cdot\dfrac{\vec{r}_{S-A}\times\left(\vec{r}\times\vec{r}_{S-A}\right)}{\left|\vec{r}_{S-A}\times\left(\vec{r}\times\vec{r}_{S-A}\right)\right|} \right| < R \end{cases} \Rightarrow \beta = 0 \tag{6}$$

with $\vec{r}$ and $\vec{r}_{S-A}$ the radius-vectors asteroid to spacecraft and Sun to asteroid respectively.

The previous model does not consider any umbra or penumbra effects, implying that SRP is either active or not. A slightly more complex model was implemented, with the lightness number varying with the shaded area of the Sun. The first condition in Eq. (6) still needs to be checked, to ensure the spacecraft is in the unlit area of the asteroid.

In order to calculate the eclipsed area of the Sun by a spherical asteroid, the intersection area of two circles (Sun and asteroid) projected at a distance of 1 AU is calculated. In order to do so, the projected radius and distance between the centres of both circles is given by:

$$R_1 = \frac{R_{SUN}}{\left|\vec{r}_{S-SC}\right|}; \quad R_2 = \frac{R}{\left|\vec{r}\right|}; \quad d = \frac{\left|\vec{r}_{S-A}\right|\left|\vec{\rho}\right|}{\left|\vec{r}_{S-SC}\right|\left|\vec{r}\right|} \tag{7}$$

where R_{SUN} is the radius of the Sun and the radial vector $\vec{\rho}$ is calculated as:

$$\vec{\rho} = \vec{r} - \left(\vec{r}\cdot\vec{r}_{S-A}\right)\frac{\vec{r}_{S-A}}{\left|\vec{r}_{S-A}\right|} \tag{8}$$

The intersection area is then given by the real part of the following expression:

$$\begin{aligned} A_{\cap} = \text{real}\Bigg(& R_1^2 \arccos\left(\frac{d^2+R_1^2-R_2^2}{2dR_1}\right) + \ldots \\ & \ldots + R_2^2 \arccos\left(\frac{d^2+R_2^2-R_1^2}{2dR_2}\right) - \ldots \\ & \ldots - \frac{1}{2}\sqrt{(-d+R_1+R_2)(d+R_1-R_2)(d-R_1+R_2)(d+R_1+R_2)}\Bigg) \end{aligned} \tag{9}$$

Finally, the new lightness number during umbra or penumbra is then calculated subtracting the ratio of the projected intersection area and the Sun area.

$$\beta^* = \beta\left(1 - \frac{A_{\cap}}{\pi R_1^2}\right) \tag{10}$$

Extensive testing shows that the difference between both models is negligible. The more complex model does not increase the computational time significantly, so it will be the one implemented except for a few cases of heavy computations.

Figure 5 and Figure 6 illustrate the importance of including eclipses in the propagation. The number of complete revolutions or the conditions of re-impact or escape vary significantly with them. For instance, in the example case plotted, if no eclipses are considered there is a final pericentre (O marker in the phase

space plot) taking place before the eccentricity grows back to critical levels, resulting in an additional revolution before impact. The same trajectory with eclipses does not clear the surface in this final pericentre passage and re-impacts 15 hours before. The phase space plot looks similar in both cases, but plotting the eccentricity (Figure 6), the three eclipse phases where the SRP is not active and the orbital element does not vary can be clearly pinpointed.

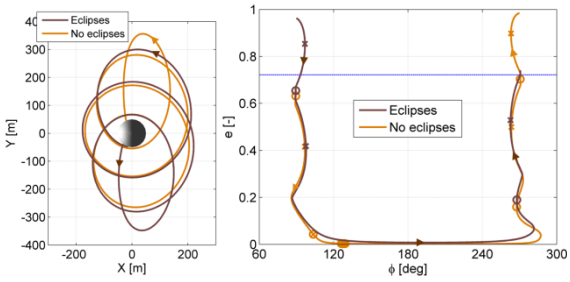

Figure 5: Differences in propagation with and without eclipses in the co-orating frame (left) and the phase space (right). Apocentres and pericentres are indicated with X and O markers respectively in the phase space. When no eclipses are considered there is an additional revolution.

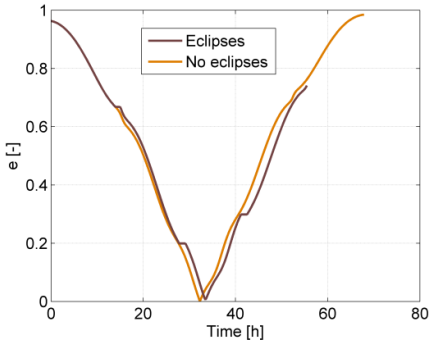

Figure 6: Eccentricity evolution with and without eclipses for an equatorial trajectory departing from the surface of the asteroid.

IV.II. Non-Equatorial Dynamics

In this paper, we will limit ourselves to equatorial trajectories with zero inclination, assuming the equator of the asteroid coincides with the orbital plane of the asteroid around the Sun. These trajectories remain in the same orbital plane, as there are no external out-of-plane forces. However, the coded propagation tools can handle 3-dimensional trajectories, and the evolution of eccentricity and phase angle follows the same pattern (eccentricity decreasing for prograde orbits with $\phi < 180^0$ and increasing for $\phi > 180^0$) for trajectories with inclinations as high as 60 degrees. The evolution of the inclination has a similar behaviour, decreasing for $\phi < 180^0$ and increasing for $\phi > 180^0$ in prograde orbits. The detailed analysis of out-of-plane movement is left here for future work.

IV.III. Higher Order Gravitational Terms

When orbiting in close proximity to an asteroid, the irregular shape and non-sphericity of their gravitational field introduces large perturbations in a spacecraft trajectory.

For the purpose of studying the influence of non-sphericity, the asteroid is modelled as a constant density tri-axial ellipsoid rotating uniformly about an axis corresponding to its maximum moment of inertia (see Figure 7 left). The ratio between the ellipsoid semi-major axes is assumed to be $\sqrt{2}$, and the total volume and mass is equal to that of a spherical asteroid of equivalent radius R. The rotation axis direction is constant and assumed aligned with the Z-axis of the co-rotating frame, and the state of the asteroid can be thus defined by a single angle γ between the X-axis of the co-rotating frame (Sun-asteroid direction) and the principal axis associated with the ellipsoid's minimum moment of inertia.

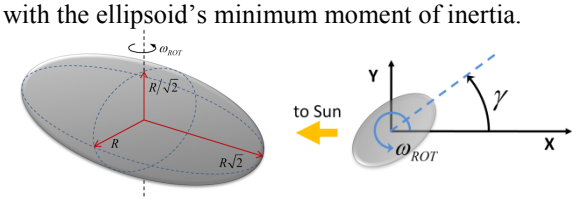

Figure 7: Tri-axial ellipsoid dimensions and angle γ definition.

With this definition of the principal axes, the moments of inertia of the ellipsoid in their principal axes are given by:

$$\begin{aligned} I_{11} &= \frac{1}{5}m\left(b^2+c^2\right) = \frac{3}{10}mR^2 \\ I_{22} &= \frac{1}{5}m\left(a^2+c^2\right) = \frac{1}{2}mR^2 \\ I_{33} &= \frac{1}{5}m\left(a^2+b^2\right) = \frac{3}{5}mR^2 \end{aligned} \tag{11}$$

with the semi-major axes $a = \sqrt{2}R$, $b = R$ and $c = R/\sqrt{2}$ as shown in Figure 7.

The gravitational field of the ellipsoid is modelled as a spherical harmonic potential for simplicity. The spherical harmonics dimensionless coefficients in the body frame up to order four can be calculated using the relations provided by Balmino (1994) as:

$$\begin{aligned} C_{20} &= \frac{1}{5R^2}\left(c^2 - \frac{a^2+b^2}{2}\right) = -\frac{1}{5} \\ C_{22} &= \frac{1}{20R^2}\left(a^2-b^2\right) = \frac{1}{20} \\ C_{40} &= \frac{15}{7}\left(C_{20}{}^2 + 2C_{22}{}^2\right) = \frac{27}{280} \\ C_{42} &= \frac{5}{7}C_{20}C_{22} = -\frac{1}{140} \\ C_{44} &= \frac{5}{28}C_{22}{}^2 = \frac{1}{2240} \end{aligned} \tag{12}$$

where the reference radius for normalisation is chosen as the mean radius of the asteroid and is equal to R.

This gravity model can be applied to any other ellipsoid or geometry of the asteroid, resulting in different trajectories. The assumption of rotation around the Z-axis results in the largest in-plane perturbations for the equatorial trajectories, which is in principle conservative. However, other rotational states not aligned with the orbit normal would additionally induce out-of plane perturbations which would in turn generate more complicated trajectories.

Figure 8 shows an example of the effect of the additional gravity terms on the evolution of two trajectories. The position of the ellipsoid is plotted at the initial time. It can be easily observed that prograde trajectories (top), which orbit in the same direction as the asteroid rotation, are much more strongly perturbed than retrograde trajectories (bottom). Prograde orbits may enter in resonance with the asteroid rotation, become hyperbolic and escape as in the example, or have dramatic changes in semi-major axis and eccentricity and prematurely impact. The eccentricity evolution in retrograde trajectories also has peculiar features, but in general they are more stable and reproduce more closely the behaviour of the spherical asteroid case.

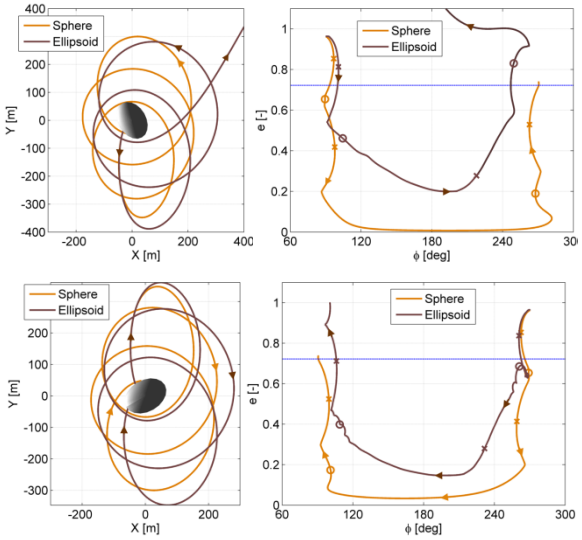

Figure 8: Differences in propagation including higher order gravitational terms in the co-rotating frame (left) and the phase space (right). Prograde trajectories (top) are much more strongly affected when compared to retrograde ones (bottom).

V. SRP ENABLED TRAJECTORIES

Using the models described above, the search for useful SRP dominated highly non-Keplerian trajectories was performed for hoppers and orbiter spacecraft around a hypothetical asteroid of 50 m radius, constant standard NEA density of 2.6 g/cm^3 (Chesley et al., 2002), and a 4 hour rotational period on a circular orbit at 1 AU around the Sun. The rotational axis is assumed perpendicular to the orbital plane, and the direction of rotation is the same as the orbit direction. The initial preliminary analysis is carried out for a spherical asteroid, and the effect of higher order gravitational harmonic terms on the generated trajectories is discussed in section V.V.

A spacecraft mass of 100 kg is assumed. Orbiting regimes will be discussed as a function of the variable effective area A instead of the lightness number, as it allows a better grasp of the spacecraft solar sail or reflective surface involved.

In order to adequately categorize the trajectories around the minor body it is useful to define a winding number as the number of revolutions that the XY projection of one trajectory on the co-rotating frame performs around the centre of the asteroid counter-clockwise from a hypothetical ejection point to its impact or escape point.

$$WN = \left(\theta(t_{end}) - \theta(t_0)\right)/2\pi \tag{13}$$

The angle θ can be measured from any arbitrary direction in the XY plane (e.g. the X-axis) and must be continuous (no jumps of ±2π). Prograde and retrograde trajectories have positive and negative winding numbers respectively.

The winding number is a more useful geometrical definition than the commonly used number of complete orbits, due to the fact that the argument of pericentre varies greatly in these types of trajectories, and they can also become parabolic or hyperbolic and invert the orbit direction. In the case of escaping parabolic or hyperbolic trajectories, trajectories are propagated until they reach 15 asteroid radii, and the winding number is calculated up to this point.

Figure 9 represents the winding number for trajectories departing vertically (relative velocity perpendicular to the surface) from a spherical asteroid with phase angle $\phi = 90^0$. Given an initial osculating semi-major axis a_0 and considering the asteroid rotational angular velocity ω_{ROT}, the corresponding initial osculating eccentricity that satisfies the vertical relative departure velocity condition is given by:

$$e_0 = \sqrt{1 - \frac{\omega_{ROT}{}^2 R^4}{\mu_A a_0}} \tag{14}$$

The condition of vertical departure can be of importance for hopper spacecraft that may preferably leave and return to the surface with no horizontal velocity with respect to it. Orbiter trajectories not intending to re-impact can in principle be calculated for any other departure condition.

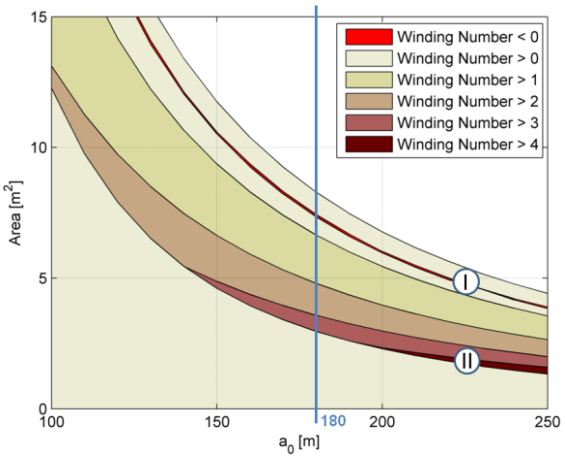

Figure 9: Winding number as a function of the initial semi-major axis and effective area, for prograde trajectories with ϕ=90 departing perpendicularly to the surface of a spherical asteroid of radius 50 m and 4 hour period of rotation.

The blank area in Figure 9 corresponds to trajectories that escape directly due to SRP and the 3rd body perturbation of the Sun before an apocentre passage takes place. The light area at the bottom contains trajectories that re-impact directly before performing a single revolution. If the SRP perturbation is large enough to ensure clearing the surface at the first pericentre passage, multiple revolution trajectories can be obtained (darker shades).

The bright red narrow area (also marked with (I)) corresponds to trajectories that crash or escape with negative winding numbers. Given that the initial conditions are for a prograde trajectory, it implies that the orbiting direction has been reversed at some point. The sensitivity to small variations in the effective area in this region and above is high. Trajectories above the red line, which perform less than one prograde revolution but have at least one apocentre passage, may re-impact or escape for small variations of the initial conditions.

If a variety of orbiting regimes with physically meaningful and realistic areas for a lightweight spacecraft are sought, a minimum semi-major axis can be selected from the previous plot.

Several trajectories of interest enabled by the SRP perturbation are described in the following sections: a hopper returning to the initial solar longitude (I), multi-revolution trajectories (II), and the study of an alternating orbiter for coverage of the sub-solar point. An initial semi-major axis of 180 m (vertical line in Figure 9) has been selected for this last case.

V.I. Hopper Free-Return Trajectories

The orbiting regime with negative winding numbers (I) requires an inversion of the orbit direction. This can only take place if the eccentricity reaches values equal to or larger than one and the orbit becomes parabolic (or hyperbolic). Exploiting this fact, it is possible to design trajectories for a hopper that departs from the surface of the asteroid, reaches parabolic escape conditions, and then returns back to the surface of the asteroid at the same solar longitude (corresponding to winding number WN~0). An example is plotted in Figure 10 for an initial semi-major axis of 225 m, returning back to the original point after over 80 hours, or more than 20 asteroid revolutions. The left figure shows also the sensitivity of the solution for this regime of high SRP perturbation, with an escape trajectory (red line) after the orbit direction inversion with the same initial conditions and only about 360 cm^2 less of effective area.

The trajectory plotted returning to the original solar longitude (blue solid line) has however a residual relative horizontal velocity when returning to the surface of the asteroid (point 2), which may not be well suited for a hopper, if sliding in the low gravity environment of the asteroid needs to be avoided.

Fine tuning the area can lead to a trajectory with a second inversion of the orbit direction (eccentricity reaching again a value of 1 at inversion) that arrives again to the surface (point 2') in a prograde orbit with the same eccentricity and phase angle as in the initial conditions, and only a vertical component of the relative velocity with respect to the surface (see Figure 11).

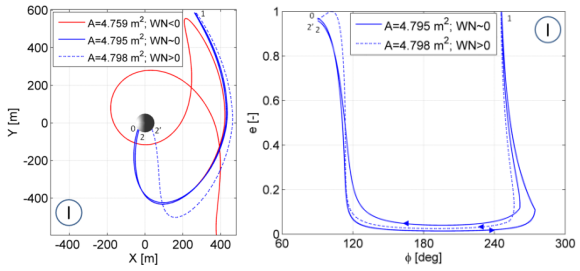

Figure 10: Example case with winding number close to 0 for a 225 m initial semi-major axis, in the co-rotating frame (left) and the phase space (right). The orbit direction is inverted when the orbit becomes parabolic (point 1). For small variations of the effective area it is possible to obtain trajectories ranging from a hopper returning to the initial solar longitude to escape trajectories.

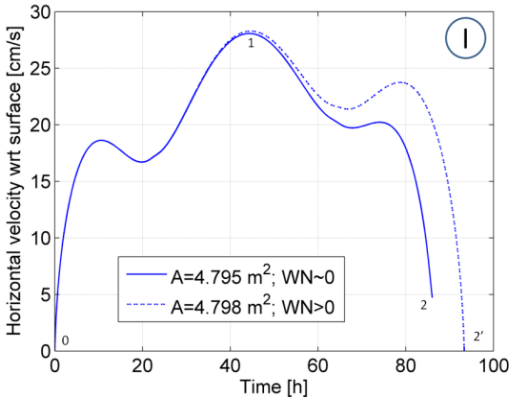

Figure 11: Horizontal velocity with respect to the asteroid surface for a returning hopper. Trajectories that depart and return vertically to the asteroid surface can be designed, i.e. trajectories that return with negligible horizontal velocity (dashed line).

V.II. Multiple revolution trajectories

Figure 12 presents an extreme case of a trajectory with close to 5 revolutions for a departure semi-major axis of 225 m (point II in Figure 9). The evolution of the eccentricity in the phase space clearly follows the predicted behaviour by the isolines of Hamiltonian in section III. Similar trajectories could be employed to observe the sub-solar point of the asteroid while at the same time improving the gravity field characterisation of the asteroid. This inspired the trajectories presented in the following section, where a spacecraft reverses the orbiting direction after a number of revolutions.

These trajectories with a high number of revolutions have the drawback of extremely close passes skimming the asteroid surface, which in a more realistic case with a full shape and gravitational model would likely result in a re-impact or large perturbations to the orbit.

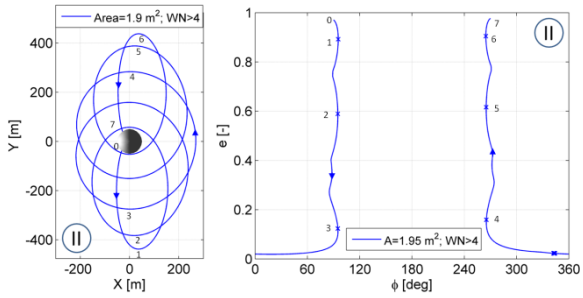

Figure 12: Illustrative case for winding number larger than 4 for a 225 m initial semi-major axis, in the co-rotating frame (left) and phase space (right). Trajectories with almost five full revolutions can be obtained. Apocentres are indicated with numbers 1-6 and markers on the right plot.

V.III. Alternating Orbiter: apocentre manoeuvres

An alternating orbiter that reverses its velocity vector with a small manoeuvre at apocentre after a number for evolutions is now presented. This interesting solution is proposed as an alternative to (non-existent) stable equatorial orbits, and would allow coverage of the sub-solar point and the whole equatorial region, as well as possibly an improvement and characterisation of the gravity field and shape model of the asteroid while at safe distances. The solution consists of symmetric single or multi-revolution trajectories that alternate prograde with retrograde orbits. The trajectories start at apocentre and perform an inversion of the velocity vector at the last apocentre before a re-impact with the surface. Trajectories similar to the one presented in the previous section could also be devised performing the inversion of the velocity vector two apocentres before re-impact (from points 2 to 5 in Figure 12).

Figure 13 presents a close-up of Figure 9 around the region of the selected semi-major axis 180 m. Symmetric trajectories with respect to the X-axis with less than 1 to 4 revolutions (O, X, triangular and square markers) have been identified as possible candidates for the alternating orbiter operational orbit. The graph includes a plot of these trajectories where the final apocentres where inversion manoeuvres take place are indicated. Manoeuvres take place from every 16 hours for the case with less than 1 revolution, up to every 53 hours for the case with close to 4 orbits.

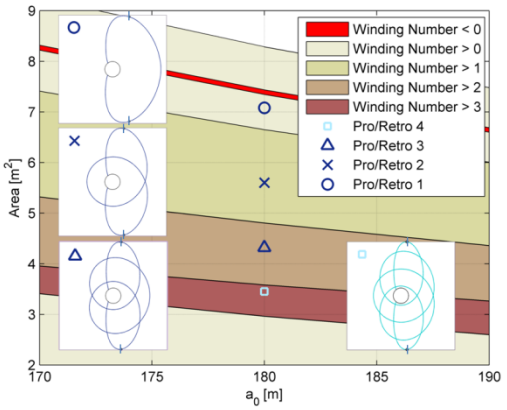

Figure 13: For any arbitrarily selected initial semi-major axis (180 m in this case) symmetric trajectories can be found with one or several revolutions. Alternating orbiter solutions with manoeuvres at the extreme apocentres allow coverage of the whole asteroid equatorial region.

The solution with almost one revolution (O marker) does not provide coverage to the sub-solar point. It could nonetheless be a possible starting safe orbit to perform the first characterisation of the

asteroid before transferring to some of the multi-revolution options. The solution with close to 4 revolutions (square marker) has again the drawback of very low altitude pericentres and may not be suitable for a realistic case.

Figure 14 presents the intermediate solutions for an alternative orbiter with over one (top, X marker) and over two (bottom, triangular marker) complete revolutions. The trajectories in the co-rotating frame (left) have been numerically propagated until the fifth inversion of the velocity with no additional control or correction manoeuvres. Key points in the orbit are indicated both in these plots and on the phase space (right), where it is possible to observe the almost symmetric behaviour of the Hamiltonian for prograde and retrograde trajectories.

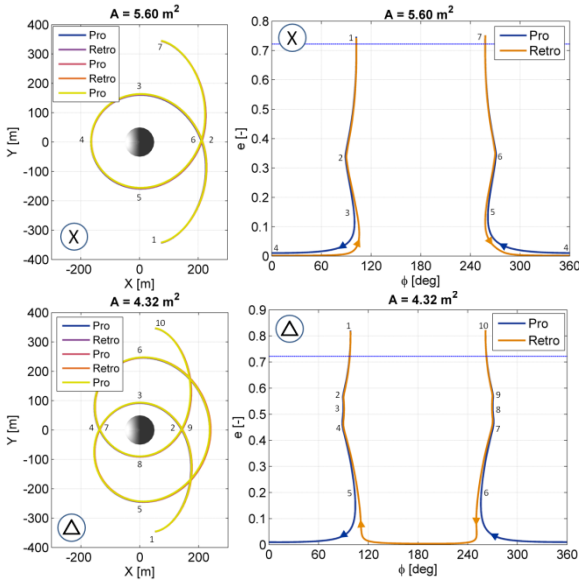

Figure 14: Two alternating orbiter solutions with more than one (top) and two (bottom) revolutions in the co-rotating frame (left) and the phase space (right). Sub-solar point is covered at distances ranging from 90 to 120 meters.

Comparison with direct hovering

The cost of the strategy proposed can be easily compared with more traditional hovering strategies. As already mentioned, the alternating orbiter solution requires small manoeuvres every 16 to 53 hours. The size of these manoeuvres is small (less than 2 cm/s for each), which would amount to a total cost over a period of one year of 2 to 10 m/s depending on the case. Missions around asteroids are unlikely to perform such long duration phases of a year, but this period was chosen as reference for comparison.

Table 1 compares the frequency and size of manoeuvres required, and the total yearly costs for three different orbit maintenance strategies.

The first case consists of continuous fixed point hovering in the co-rotating frame at a constant distance over the sub-solar point. In this strategy there are no manoeuvres per se but a constant acceleration needs to be applied. The total costs over a full year of hovering would be of the order of 50 m/s for a hovering point 200 m above the sub-solar point for an assumed effective area of the spacecraft of 3 m^2, 130 m/s if the distance is halved. The required ΔV changes slightly with the area, but even assuming no SRP the yearly hovering costs would be over 40 m/s for the 200 m distance point.

The second set of results corresponds to a simple box control hovering strategy, in which the velocity is reversed every time the spacecraft falls below a certain height. This is a simplified version of the strategy proposed in Scheeres (2012). Two semi-major axes and three different box lower limit heights have been selected. The eccentricity is calculated with Eq. (14), that is, the shape of the orbits selected is similar to the ones used in the alternating orbiter. No SRP perturbation has been taken into account to estimate the frequency and size of the manoeuvres (Keplerian propagation is assumed). Depending on the selected parameters, the size of the manoeuvres ranges from 1.7 to 3.6 cm/s and one manoeuvre is required every 7 to 13 hours. The total accumulated costs over one year would be equivalent to 16 to 31 m/s, lower than the fixed point hovering.

Finally, the estimated costs over a year are presented for the alternating orbiter solution and the 4 cases as a function of the number of revolutions. The manoeuvre size is smaller than the previous case, as all manoeuvres are performed at apocentre, and the frequency is also lower: manoeuvres need to take place only every 16 to 53 hours. The total cost over one year is thus reduced. In the two intermediate cases of interest presented in Figure 14, the total ΔV over one year will be between 2.8 and 5.0 m/s.

	a_0 [m]	A [m^2]	Time man. [h]	ΔV One man. [cm/s]	ΔV Year [m/s]
Hover fix H=100 m	150	3.00	cont.	(acceleration 4.2 10^{-4} cm/s^2)	131.64
Hover fix H=200 m	250	3.00	cont.	(acceleration 1.6 10^{-4} cm/s^2)	50.10
Hover Box H>50 m	150	N/A	9.6	3.48	31.92
	180	N/A	12.9	3.62	24.56
Hover Box H>100 m	150	N/A	8.6	2.46	25.22
	180	N/A	12.0	2.66	19.44
Hover Box H>150 m	150	N/A	7.1	1.74	21.35
	180	N/A	10.7	2.01	16.41
Altern Orbit <1 rev	180	7.08	16	1.92	10.52
Altern Orbit <2 rev	180	5.60	28	1.61	5.04
Altern Orbit <3 rev	180	4.32	42	1.36	2.84
Altern Orbit <4 rev	180	3.45	53	1.20	1.98

Table 1: Frequency and size of manoeuvres required for each type of control

The benefits of such a strategy are not only lower fuel and operational costs, but also the possibility of coverage of other points along the equator (anti-solar point, terminator crossings…), the variation in height over distinct passes, and possibly a better determination of the gravity field and shape model of the asteroid.

V.IV. Alternating Orbiter: closed unstable solutions

Motivated by the natural inversion of the orbit direction that takes place for areas in the red "chaotic" region in Figure 9, when orbits turn parabolic, a search was performed for solutions that performed 2 or more of these natural inversions and return to the initial point. If such solutions exist they will represent closed periodic orbits in the equator of the asteroid that perform part of the rotation in prograde direction and part in retrograde direction.

We assumed a symmetric solution and resorted thus to a search of trajectories starting at a defined point on the X-axis x_0, with an initial velocity with only a single component in the Y-axis v_y. This velocity and the effective area were optimised to find periodic solutions. Figure 15 presents one such solution for an initial x_0 of 345 m. The total period of the orbit is 67.2 hours and the spacecraft spends over 12 hours at altitudes lower than 160 m. Another interesting characteristic of this solution in particular is that it performs the inner loop in a retrograde direction, and the outer loop in a prograde direction. This hints at the possibility of finding similar orbits in a more complex model with non-sphericity perturbation, as retrograde orbits were least affected.

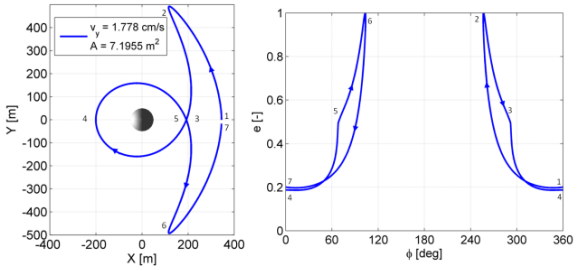

Figure 15: Unstable closed orbiter solution in the co-rotating frame (left) and phase space (right) with two orbiting direction inversions (points 2 and 6)

These solutions are though unstable orbits. The reason is that even if the initial conditions are matched for x_0 and v_y, there is always a residual velocity in the X-direction v_x that unless eliminated causes a divergence from the original trajectory after 2 revolutions. This residual velocity is though of the order of 0.01 cm/s, so if fine control strategies are applied (either by introducing trajectory correction manoeuvres every revolution or by fine-tuning a non-constant effective area), the orbit could be maintained at low costs. Trajectories are also very sensitive to small variations in the effective area. Figure 16 shows the result of propagation of the previous trajectory until re-impact or escape, with effective areas differing only by 1 cm^2. The second revolution does not match the initial conditions at the Y-axis crossing and during the third revolution the SC either re-impacts or escapes.

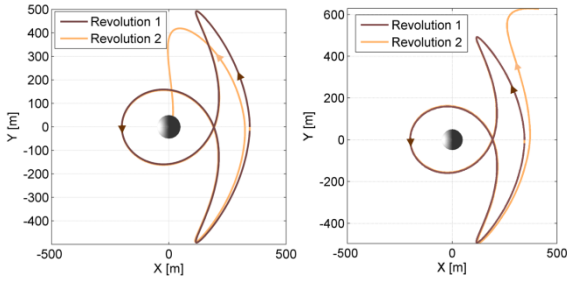

Figure 16: Small variations in the area (1 cm^2) cause large deviations from the closed orbit after the second revolution, from impact to escape.

Additional symmetric solutions were found with two inversions but no inner revolution around the asteroid, and with 4 inversions and multiple low-altitude passes.

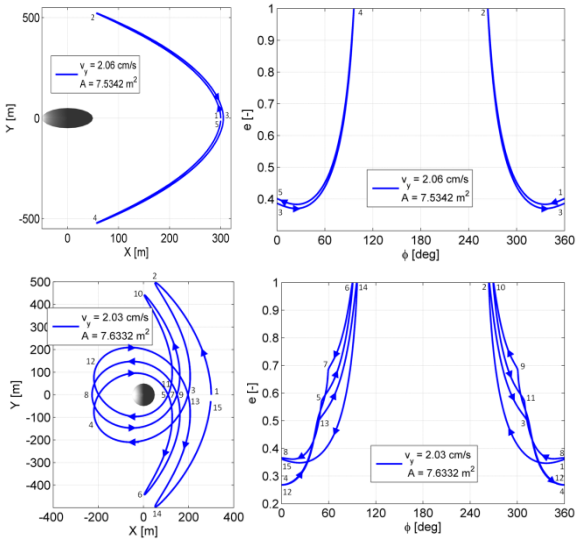

Figure 17: Unstable orbiter solutions with initial x_0 of 300 m, in the co-rotating frame (left) and phase space (right) with two orbit direction inversions at points 2 and 4 and no loops (top), and with four orbit direction inversions (points 2, 6, 10 and 14) and multiple low altitude passages (bottom)

The first solution (Figure 17 top) is not of interest for the sub-solar coverage case, and it provides no obvious advantage with respect to stable terminator orbits (unless direct coverage of the anti-solar point is required). It may well be a special case of the trajectories contained inside paraboloids described by Bookless (2006) or Broschart (2013). The aspect ratio between axes was modified in the co-rotating frame

for this plot to differentiate retrograde and prograde phases.

The second solution (Figure 17 bottom) has low-altitude passes in the prograde direction that would probably render it unstable with a more complex gravitational model of the asteroid. Their trajectories have nevertheless been plotted here in Figure 17 to illustrate the wide range of possible solutions to the problem.

V.V. Introduction of Higher Order Gravitational Harmonics: Effect on Alternating Orbiter

In this section the possibility of designing alternating orbiter solutions for non-spherical asteroids is considered. Contrary to the case of the point mass or spherical mass distribution, for any irregular shape the effective areas required to perform a trajectory with a certain winding number, or number of revolutions, varies with the initial attitude of the asteroid. For the tri-axial ellipsoid model described in section IV.III, the winding number for an osculating departure a_0 of 180 m is plotted for different initial γ (defined in Figure 7) for a retrograde orbiter (top) and prograde orbiter (bottom). The retrograde orbits are more stable as expected, with wide variations in the prograde orbit for winding numbers larger than 2 for small changes in the initial attitude of the asteroid.

The symmetric solutions with more than one revolution that were the basis for the alternating orbiter strategy have been indicated with markers for the retrograde case. In the prograde case only solutions with less than two revolutions can be guaranteed to exist for a wide range of initial conditions.

It is nonetheless possible to combine a retrograde solution with close to 3 revolutions, with a prograde one of close to two. This maximizes the number of passes over the sub-solar point (2+1) while avoiding the chaotic behaviour introduced when prograde orbits enter in resonance with the rotation of the asteroid. The effective areas required for each phase would be different however. Figure 19 indicates the required areas for the proposed solutions with a 3-revolution retrograde orbit (black triangular marker), and the associated return 2-revolution prograde orbit (black X marker). The ratio between both areas is of the order of 1.6.

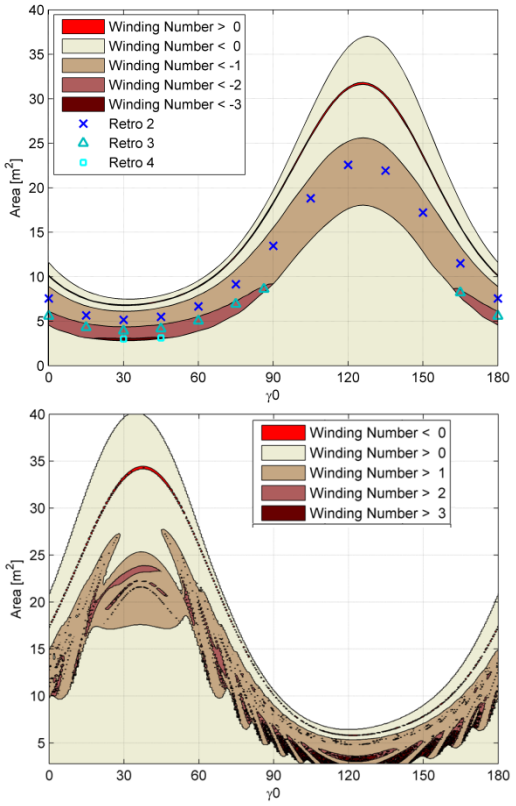

Figure 18: Winding number for a retrograde orbiter (top) and a prograde orbit (bottom) around a rotating ellipsoid, as a function of the initial relative geometry and the area. Symmetric solutions for the retrograde case are indicated with markers.

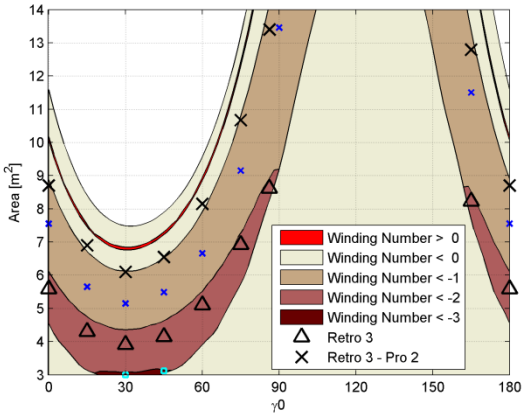

Figure 19: Proposed solution for an alternating orbiter combining a 3 revolution retrograde orbit (black triangular markers) and a 2 revolution prograde orbit (black X markers)

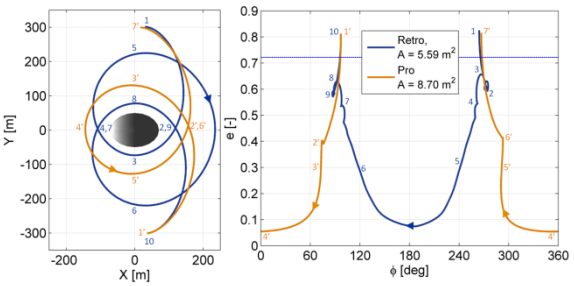

Figure 20: Alternating orbiter for the 3-retrograde / 2-prograde case with an initial γ angle of zero degrees. Plots in co-rotating frame (left) and phase space (right)

The time between manoeuvres performed at apocentre to reverse the velocity vector is also different for each of the two phases. Figure 20 plots one particular case for a starting γ of zero in the co-rotating frame and the phase space. The ellipsoid is plotted at the initial time. The prograde orbit is always further away from the surface of the asteroid to avoid undesired escape or re-impact. Two manoeuvres of size 1.52 cm/s are required every 59 hours (one after 36.0, the other after 22.6 hours). This would amount to a yearly cost of 4.47 m/s.

Another example solution has been propagated in Figure 21 until the fifth velocity inversion for a different starting γ of 60 degrees. The areas required in this case are 5.1 m^2 and 8.15 m^2 for retrograde and prograde orbits respectively; and two manoeuvres of similar size (1.5 cm/s) are required every 56 hours. There has not been any fine control trying to reduce the errors by modifying the manoeuvres at subsequent apocentre passages. The areas are also kept constant for the two orbiting directions. If finer control is desired, the manoeuvre size and direction could be optimised and the areas could be tuned each revolution to stay as close as possible to the nominal original trajectory with minor extra ΔV costs.

Depending on the initial state of the asteroid the size of the manoeuvres ranges from 1.2 to 1.8 cm/s, the total duration of a retro-pro phase can be from 40 to 70 hours and the yearly costs are in the range of 3 to 8 m/s.

Orbiter solutions with natural inversions of the orbit direction at the parabolic eccentricity have also been found for the tri-axial ellipsoid model. The area required varies slightly with the asteroid's initial attitude (see Figure 22), and an active control with varying area would be desired to keep the orbit stable. The analysis of an optimal control is left for future work.

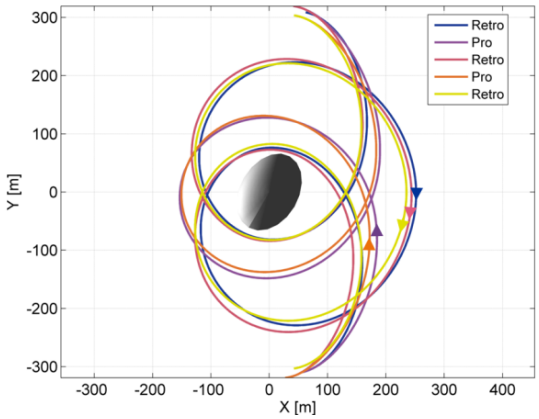

Figure 21: Multiple velocity inversions for an alternating orbiter for the 3-retrograde / 2-prograde case with an initial γ angle of 60 degrees.

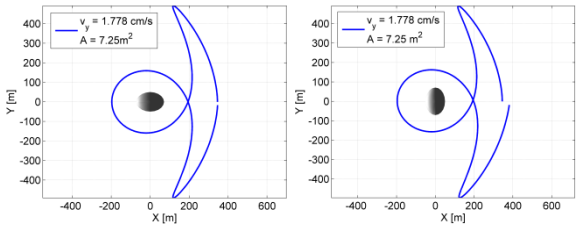

Figure 22: Differences in the Y-axis crossing for the same starting state vector for two different initial asteroid attitudes.

VI. SOLUTIONS FOR SYSTEM IMPLEMENTATION

In the previous sections, solutions that require varying effective areas depending on the initial conditions and the orbit direction have been described. We try to justify the feasibility of such variable area systems with current technologies.

The ratio of the areas required for the 3-revolution retrograde and the 2-revolution prograde orbits presented in section V.V is of the order of 1.6. A system with varying areas of this order could be implemented in multiple ways (see Figure 23). Various variable effective area solutions include (but are not limited to): solar panels of varying orientation with respect to the Sun (a) (e.g., an α angle of 50 deg would provide the required ratio of 1.6), additional deployable solar panels as shown in solution (b), or complex variable geometry sails such as the quasi-rhombic pyramid proposed by Ceriotti et al. (2013) (c)

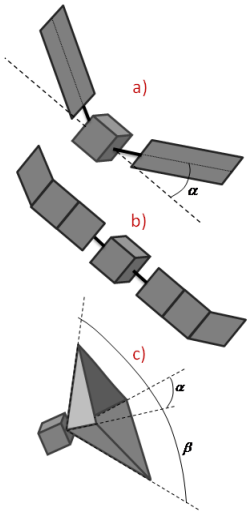

Figure 23: Variable effective surface mechanisms. Tilting panels (a), additional deployable panels (b), or varying quasi-rhombic pyramidal configuration (c).

Most of these systems have a stable equilibrium attitude with respect to the Sun: the slanted surfaces point away from the Sun direction while the bus remains Sun-pointing. This self-stabilising attitude would need to be taken into consideration when designing the spacecraft, in particular for the location of radiators and Sun-shields, and for the payload enclosures. In the example of the quasi-rhombic pyramid, visual spectrum cameras inside the pyramid would allow observing the illuminated faces of the asteroid while they would face away from it when in the dark side. Additional visual and/or IR cameras may be required in the lateral faces in order to observe the unlit areas of the asteroid. The small thrusters required to alternate the orbiting direction of the spacecraft need always to thrust in the Sun direction, which also constrains their location in the spacecraft.

Up to this point we have considered the reflectivity or solar pressure parameter Q=1, corresponding to a perfectly absorbing surface. An alternative to variable effective area is to modify in a controlled way the SRP perturbation through the use of reflective surfaces coated with electro-chromic material than can vary its reflectivity when an electrical current runs through it (schematic in Figure 24). The benefit of such an approach is a faster and more flexible variation of the SRP effect that removes the risk of having movable parts. It may even allow attitude control by selective variation of the reflectivity across the surface (Borggräfe et al., 2013). Current electro-chromic devices such as the patches used in the Ikaros solar sail demonstrated a variation in the reflectivity by a factor of 1.4 (Funase et al., 2010), which is close to the desired values.

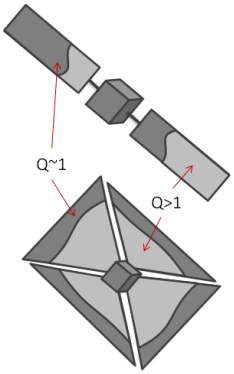

Figure 24: Variable reflectivity through electro-chromic coatings modifies the SRP perturbation without changing the area.

In practise, a combination of both variable surface and variable reflectivity may be required. A variable surface would be useful to account for the great uncertainties in the geometry and gravity field of such small bodies before the close approach, and until proper characterisation of the target body is complete. Variable reflectivity devices would still be required for faster modifications once the characterisation is complete, and for fine control. The variations required by the alternating orbiter trajectories between prograde and retrograde orbits presented here could be provided by the electro-chromic devices, while larger variations depending on the orbit geometry with respect to the body axes would be preformed with a variable area mechanism.

VII. CONCLUSIONS AND FUTURE WORK

Proximity phases for spacecraft around small minor bodies are highly perturbed by the solar radiation pressure (SRP) perturbation. Stable orbits that allow a proper coverage of the sub-solar point are limited or non-existent.

This paper proposed solutions to circumvent that problem, allowing coverage of the region in the orbital plane of the asteroid, including the sub-solar and anti-solar points. The strategies presented combined retrograde and prograde orbits and take advantage of the natural evolution of the orbit eccentricity to reduce the size and frequency of manoeuvres required when compared to more traditional hovering strategies. These strategies require a variation of the effective area of the spacecraft, depending on the desired trajectories, the asteroid characteristics, or the initial conditions. Possible implementations of variable area spacecraft are discussed.

Additional solutions of interest are presented, including possible free return trajectories for hopper spacecraft, and semi-stable periodic closed orbits that

benefit from inversions of the orbit direction due to the natural dynamics.

The trajectories presented have been generated in the photo-gravitational circular restricted 3-body problem assuming a tri-axial ellipsoid shape for the asteroid. Further work is required to check the stability of these orbits, in particular with more irregular gravity fields. So far only planar orbits limited to the orbital plane of the asteroid have been studied. A full problem extension to out-of-plane dynamics is left for future work. Active control strategies have not been implemented or discussed in detail.

VIII. ACKNOWLEDGEMENTS

The work reported was supported by European Research Council grant 227571 (VISIONSPACE).

REFERENCES

BALMINO, G. 1994. Gravitational Potential Harmonics from the Shape of an Homogeneous Body. *Celestial Mechanics and Dynamical Astronomy,* 60**,** 331-364.

BOOKLESS, J. & MCINNES, C. 2006. Dynamics and Control of Displaced Periodic Orbits Using Solar-Sail Propulsion. *Journal of Guidance, Control and Dynamics,* 29**,** 527-537.

BOOKLESS, J. P. 2006. *Dynamics, Stability and Control of Displaced Non-Keplerian Orbits.* PhD thesis, University of Glasgow.

BORGGRÄFE, A., HEILIGERS, J., CERIOTTI, M. & MCINNES, C. R. 2013. Distributed Reflectivity Solar Sails for Extended Mission Applications. *3rd International Symposium on Solar Sailing.* Glasgow, UK.

BROSCHART, S. B., LANTOINE, G. & GREBOW, D. J. 2013. Characteristics of Quasi-Terminator Orbits Near Primitive Bodies. *23rd Space Flight Mechanics Meeting.* Lihue, Kauai, USA.

BROSCHART, S. B. & SCHEERES, D. J. 2005. Control of Hovering Spacecraft Near Small Bodies: Application to Asteroid 25143 Itokawa. *Journal of Guidance, Control and Dynamics,* 28**,** 343-354.

BROSCHART, S. B. & SCHEERES, D. J. 2007. Boundedness of Spacecraft Hovering Under Dead-Band Control in Time-Invariant Systems. *Journal of Guidance, Control and Dynamics,* 30**,** 601-610.

BYRAM, S. M. & SCHEERES, D. J. 2008. Spacecraft Dynamics in the Vicinity of a Comet in a Rotating Frame. *AIAA/AAS Astrodynamics Specialist Conference.* Hololulu, Hawaii, USA.

CERIOTTI, M., HARKNESS, P. & MCROBB, M. 2013. Variable-geometry solar sailing: the possibilities of the quasi-rhombic pyramid. *3rd International Symposium on Solar Sailing.* Glasgow, UK.

CHERNIKOV, Y. A. 1970. The Photogravitational Restricted Three-body Problem. *Soviet Astronomy - AJ,* 13**,** 176-181.

CHESLEY, S. R., CHODAS, P. W., MILANI, A., VALSECCHI, G. B. & YEOMANS, D. K. 2002. Quantifying the Risk Posed by Potential Earth Impacts. *Icarus,* 159**,** 423-432.

COLOMBO, C., LÜCKING, C. & MCINNES, C. R. 2011. Orbital dynamics of high area-to-mass ratio spacecraft under the influence of J2 and solar radiation pressure. *62nd International Astronautical Congress.* Cape Town, South Africa.

DANKOWICZ, H. 1993. Some special orbits in the two-body problem with radiation pressure. *Celestial Mechanics and Dynamical Astronomy,* 58**,** 353-370.

FUNASE, R., MORI, O., TSUDA, Y., SHIRASAWA, Y., SAIKI, T., MIMASU, Y. & KAWAGUCHI, J. 2010. Attitude control of IKAROS solar sail spacecraft and its flight results. *61st International Astronautical Congress 2010.* Prague, Czech Republic.

HAMILTON, D. P. & KRIKOV, A. V. 1996. Circumplanetary Dust Dynamics: Effects of Solar Gravity, Radiation Pressure, Planetary Oblateness, and Electromagnetism. *Icarus,* 123**,** 503-523.

MCINNES, C., MACDONALD, M., ANGELOPOLOUS, V. & ALEXANDER, D. 2001. Geosail: Exploring the Magnetosphere Using a Small Solar Sail. *Journal of Spacecraft and Rockets,* 38**,** 622-629.

OYAMA, T., YAMAKAWA, H. & OMURA, Y. 2008. Orbital Dynamics of Solar Sails for Geomagnetic Tail Exploration. *Journal of Spacecraft and Rockets,* 45**,** 316-323.

SCHEERES, D. J. 1994. Dynamics about Uniformly Rotating Triaxial Ellipsoids: Application to Asteroids. *Icarus,* 110**,** 225-238.

SCHEERES, D. J. 2007. Orbit Mechanics About Small Asteorids. *20th International Symposium on Space Flight Dynamics.* Annapolis, Maryland, USA.

SCHEERES, D. J. 2012. Controlled Hovering Motion at an Asteroid. *Orbital Motion in Strongly Perturbed Environments: Applications to Asteroid, Comet and Planetary Satellite Orbiters.* Springer-Verlag Berlin Heidelberg.

SCHEERES, D. J., MILLER, J. K. & YEOMANS, D. K. 2003. The Orbital Dynamics Environment of 433 Eros: A Case Study for Future Asteroid Missions. *IPN Progress Report 42-152.*

SCHUERMAN, D. W. 1980. The restricted three-body problem including radiation pressure. *The Astrophysical Journal,* 238**,** 337-342.

SIMMONS, J. F. L., MCDONALD, A. J. C. & BROWN, J. C. 1985. The restricted 3-body problem with radiation pressure. *Celestial Mechanics,* 35**,** 145-187.

TAKAHASHI, Y. & SCHEERES, D. J. 2011. Small-Body Postrendezvous Characterisation via Slow Hyperbolic Flybys. *Journal of Guidance, Control and Dynamics,* 34**,** 1815-1827.